CM² MAGAZINE

第 105 期

南方科技大学海洋磁学中心主编

http://cm2.sustech.edu.cn/

创刊词

海洋是生命的摇篮，是文明的纽带。地球上最早的生命诞生于海洋，海洋里的生命最终进化成了人类，人类的文化融合又通过海洋得以实现。人因海而兴。

人类对海洋的探索从未停止。从远古时代美丽的神话传说，到麦哲伦的全球航行，再到现代对大洋的科学钻探计划，海洋逐渐从人类敬畏崇拜幻想的精神寄托演变成可以开发利用与科学研究的客观存在。其中，上个世纪与太空探索同步发展的大洋科学钻探计划将人类对海洋的认知推向了崭新的纬度：深海（deep sea）与深时（deep time）。大洋钻探计划让人类知道，奔流不息的大海之下，埋藏的却是亿万年的地球历史。它们记录了地球板块的运动，从而使板块构造学说得到证实；它们记录了地球环境的演变，从而让古海洋学方兴未艾。

在探索海洋的悠久历史中，从大航海时代的导航，到大洋钻探计划中不可或缺的磁性地层学，磁学发挥了不可替代的作用。这不是偶然，因为从微观到宏观，磁性是最基本的物理属性之一，可以说，万物皆有磁性。基于课题组的学科背景和对海洋的理解，我们对海洋的探索以磁学为主要手段，海洋磁学中心因此而生。

海洋磁学中心，简称 CM^2，一为其全名“Centre for Marine Magnetism”的缩写，另者恰与爱因斯坦著名的质能方程 $E = MC^2$ 对称，借以表达我们对科学巨匠的敬仰和对科学的不懈追求。

然而科学从来不是单打独斗的产物。我们以磁学为研究海洋的主攻利器，但绝不仅限于磁学。凡与磁学相关的领域均是我们关注的重点。为了跟踪反映国内外地球科学特别是与磁学有关的地球科学领域的最新研究进展，海洋磁学中心特地主办 CM^2 Magazine，以期与各位地球科学工作者相互交流学习、合作共进！

“海洋孕育了生命，联通了世界，促进了发展”。21 世纪是海洋科学的时代，由陆向海，让我们携手迈进中国海洋科学的黄金时代。

目录

1. 寒武纪大爆发对地球深部碳循环的扰动

翻译人：刘宇星 11811211@mail.sustech.edu.cn

Giuliani, A., Drysdale, R. N., Woodhead, J. D., et al. ***Perturbation of the deep-Earth carbon cycle in response to the Cambrian Explosion****[J] Science Advance,2022, 8(9), eabj1325.*

https://www.science.org/doi/10.1126/sciadv.abj1325

摘要：地球碳循环受到沉积物向地幔俯冲的强烈影响。沉积俯冲物质的组成在地球历史上发生了很大变化，但这些变化对地幔碳循环的影响尚不清楚。本文，我们揭示了金伯利岩浆的碳同位素在显生宙记录了其深部地幔源组成的根本变化。约 250 Ma 前金伯利岩的 $^{13}C/^{12}C$ 保留了典型的地幔值，而较年轻的金伯利岩表现出较低和更多变的比例——这一转变与公认的金伯利岩浆作用高峰期相吻合。我们将这些变化归因于寒武纪大爆发后海洋沉积物中的有机碳含量显著增加，从而更多具有低 $^{13}C/^{12}C$ 的有机碳被俯冲带入深部。这些观测结果表明，地球表面的生物地球化学过程对深层地幔具有深远的影响，揭示了深层和浅层碳循环之间的整体联系。

ABSTRACT: Earth's carbon cycle is strongly influenced by subduction of sedimentary material into the mantle. The composition of the sedimentary subduction flux has changed considerably over Earth's history, but the impact of these changes on the mantle carbon cycle is unclear. Here, we show that the carbon isotopes of kimberlite magmas record a fundamental change in their deep-mantle source compositions during the Phanerozoic Eon. The $^{13}C/^{12}C$ of kimberlites before ~250 Ma preserves typical mantle values, whereas younger kimberlites exhibit lower and more variable ratios—a switch coincident with a recognized surge in kimberlite magmatism. We attribute these changes to increased deep subduction of organic carbon with low $^{13}C/^{12}C$ following the Cambrian Explosion when organic carbon deposition in marine sediments increased significantly. These observations demonstrate that biogeochemical processes at Earth's surface have a profound influence on the deep mantle, revealing an integral link between the deep and shallow carbon cycles.

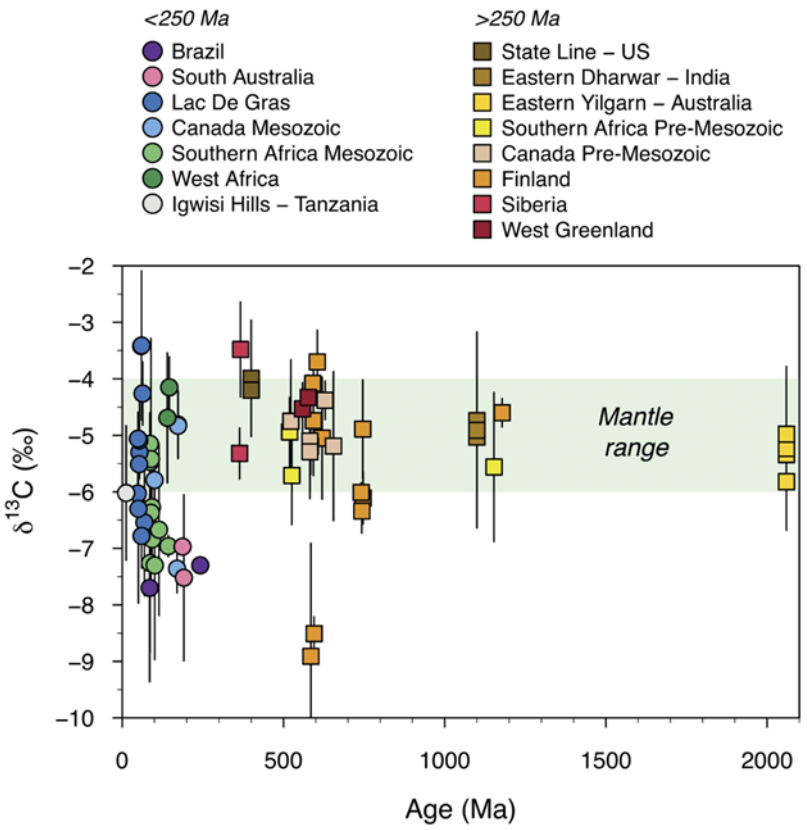

Figure 1. Carbon-isotope compositions of kimberlites and aillikites through time. Each data point represents the average of multiple analyses of ⩾3 samples, and error bars indicate the SD of the mean (see table S2). The green bar shows the carbon- isotope composition of the ambient mantle ($\delta^{13}C = -5 \pm 1‰$).

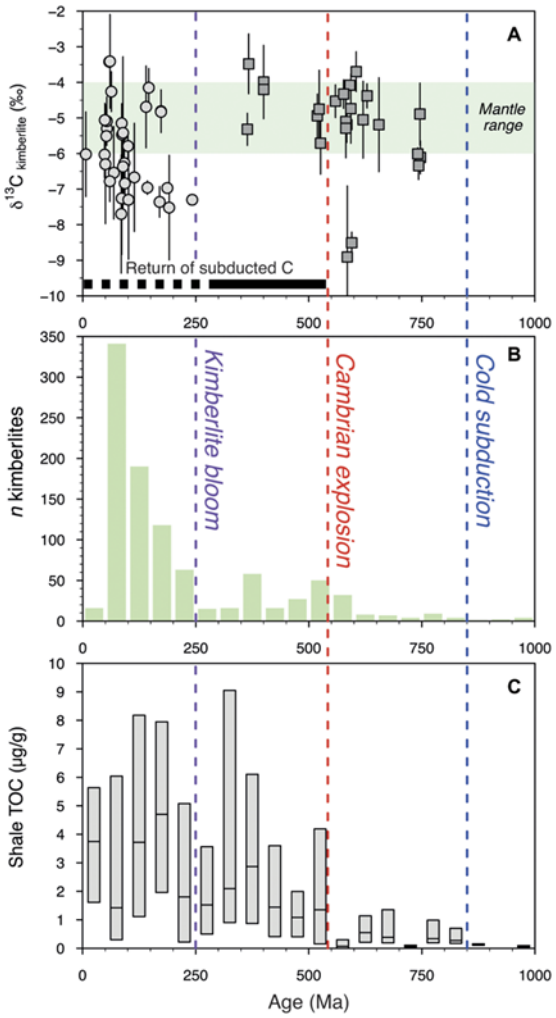

Figure 2. Comparison of kimberlite carbon-isotope compositions, frequency of kimberlite events, and total organic carbon contents in shales in the last 1000 Ma. (A) Kimberlite and aillikite $\delta^{13}C$ versus time (taken from Fig. 1). (B) Number of kimberlite events every 50 Ma [compilation of (*19*)]. (C) Boxplot showing the variability of total organic carbon (TOC) in shales binned into 50-Ma intervals [compilation of (*52*)]. Each box is delimited by the first and third quartile, and the horizontal line represents the median value. The ages of major events of geological significance for this work are highlighted, i.e., start of present-day cold subduction after ~850 Ma (*38*), the Cambrian explosion at ~542 Ma, and the kimberlite "bloom" at ~250 Ma. The horizontal black bar shows the time (≥260 Ma) required for sub- ducted material to return to the surface via magmatism related to deep-mantle plumes (*54*). Entrainment of sedimentary material containing isotopically light organic carbon, which was subducted after the Cambrian Explosion, is consistent with a wider spread in kimberlite $\delta^{13}C$ values and increased frequency of kimberlite events after 250 Ma.

2. 深水流入在始新世-渐新世过渡时期减缓了南极西部近海冰盖的扩张

翻译人：王敦繁 Dunfan-w@foxmail.com

Neben G U, Gohl K, Hochmuth K, et al. ***Deep water inflow slowed offshore expansion of the West Antarctic Ice Sheet at the Eocene-Oligocene transition****[J]. Communications earth & environment. 2022.*

https://doi.org/10.1038/s43247-022-00369-x

摘要：南极西部冰盖的稳定性受到温暖的环极地深水的入侵的影响，这些深水通过跨大陆架槽向南流向那里的海岸并融化着冰架。然而，这种海洋侵蚀对南极西部冰盖演化的影响仍然知之甚少。本文利用单道和多道地震反射剖面研究了阿蒙森海湾陆架沉积物的结构。我们估计该沉积体的形成时代大约是在始新世-渐新世过渡时期，并发现它具有灰泥沉积流的几何形状和沉积模式。我们认为，这表明深水向南流入并可能提供了热量，因此，在这个时候阻止了南极西部冰盖向海岸以外推进。我们的结论是，南极西部冰盖自最初形成以来，很可能经历了强大的海洋对其动力学的影响

ABSTRACT: The stability of the West Antarctic Ice Sheet is threatened by the incursion of warm Circumpolar Deepwater which flows southwards via cross-shelf troughs towards the coast there melting ice shelves. However, the onset of this oceanic forcing on the development and evolution of the West Antarctic Ice Sheet remains poorly understood. Here, we use single- and multichannel seismic reflection profiles to investigate the architecture of a sediment body on the shelf of the Amundsen Sea Embayment. We estimate the formation age of this sediment body to be around the Eocene-Oligocene Transition and find that it possesses the geometry and depositional pattern of a plastered sediment drift. We suggest this indicates a southward inflow of deep water which probably supplied heat and, thus, prevented West Antarctic Ice Sheet advance beyond the coast at this time. We conclude that the West Antarctic Ice Sheet has likely experienced a strong oceanic influence on its dynamics since its initial formation.

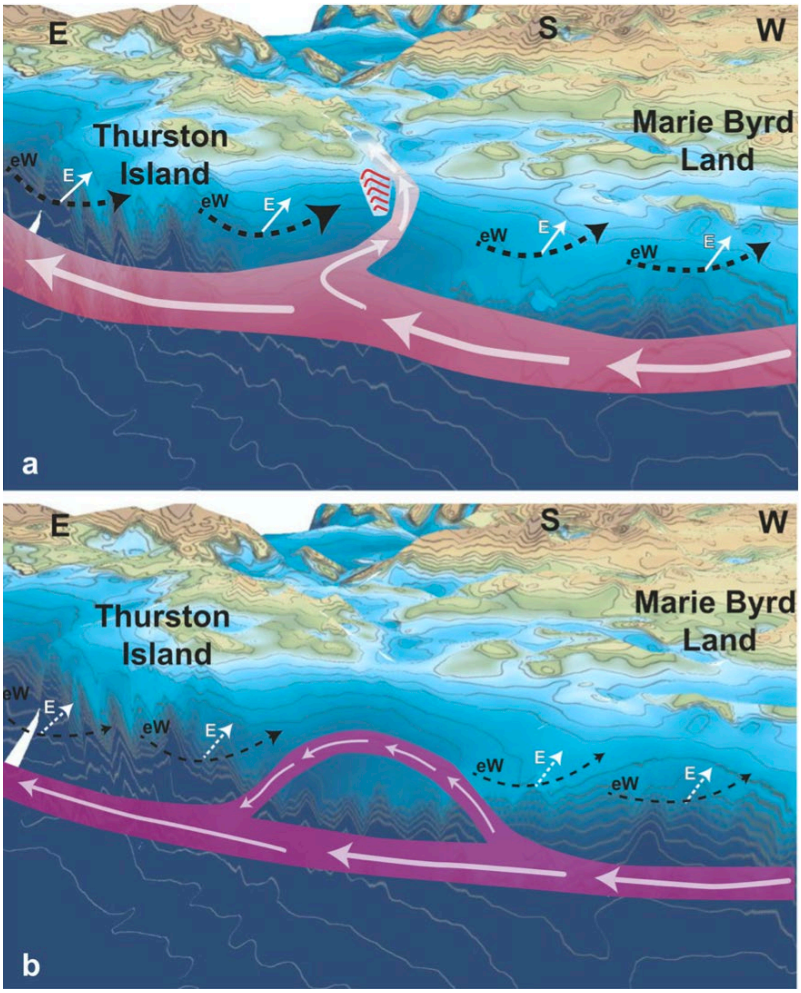

Figure 1. Conceptual model for the upwelling of deep water onto the ASE shelf in EOT. a The minimum reconstruction of the palaeotopography/ palaeobathymetry for 34 Ma shows a trough mouth or canyon in the shelf break22,41,82, which enables the intrusion of deep water (rose arrows) onto the shelf as the result of southward Ekman transport (white E, white arrow) within the easterly winds (eW). The southward flow of deep water is steered by the higher topography on the eastern ASE shelf and shapes the sediment drift (red lines). b Later in the Oligocene, increasing global cooling will have relocated the wind system (eW) northwards and influenced the intensity of upwelling. Deep water (purple arrows) now can only upwell into the outer trough and is recirculated back into the deeper ocean. This may have ended the formation of the observed sediment drift plastered against seismic horizon ASS-u2 below the eastern flank of the present-day PIT. eW= easterly winds, E, S, W = East, South, West.

3. 在过去 40 万年里多种古人类迁移到亚洲西南地区

翻译人：仲义 zhongy@sustech.edu.cn

Groucutt H S, White T S, Scerri E M, et al. ***Multiple hominin dispersals into Southwest Asia over the past 400,000 years*** *[J] Nature, 2021, 597, 376-380.*

https://doi.org/10.1038/s41586-021-03863-y

摘要：更新世时期的古人类走出非洲又返回非洲，期间必然穿越了多种多样充满挑战的亚洲西南部地区。来自地中海东部林区的考古和古生物学记录显示了主要的生物和文化转变，例如智人和尼安德特人的交替迁徙。然而，对于晚第四纪亚洲西南地区广阔的干旱地区的文化、生物和环境记录仍然缺乏，限制了我们对于区域尺度上古人类群落和行为习惯改变的深入研究。本文中，作者报道了一系列的具有年代学意义的古湖泊序列，涉及从尼孚德沙漠的石器工具组合和脊椎动物化石。这些发现包括阿拉伯地区最古老的古人类活动，揭示了至少五次的古人类向阿拉伯内陆扩张，这与大约 400、300、200、130-75 和 5.5 万年前干旱减少的短暂“绿色”气候环境相吻合。每个占领阶段都以独特的物质文化形式为特征，表明不同种群古人类群体居住，而亚洲西南部人类群落长期居住。在非洲和欧亚古人类群落被更新世撒哈拉-阿拉伯干旱环境所区分，结果揭示了气候调节的扩散和混合窗口的速度和特征。

ABSTRACT: Pleistocene hominin dispersals out of, and back into, Africa necessarily involved traversing the diverse and often challenging environments of Southwest Asia. Archaeological and palaeontological records from the Levantine woodland zone document major biological and cultural shifts, such as alternating occupations by Homo sapiens and Neanderthals. However, Late Quaternary cultural, biological and environmental records from the vast arid zone that constitutes most of Southwest Asia remain scarce, limiting regional-scale insights into changes in hominin demography and behaviour1,2,5. Here we report a series of dated palaeolake sequences, associated with stone tool assemblages and vertebrate fossils, from the Khall Amayshan 4 and Jubbah basins in the Nefud Desert. These fndings, including the oldest dated hominin occupations in Arabia, reveal at least fve hominin expansions into the Arabian interior, coinciding with brief ‘green’ windows of reduced aridity approximately 400, 300, 200, 130–75 and 55 thousand years ago. Each occupation

phase is characterized by a distinct form of material culture, indicating colonization by diverse hominin groups, and a lack of long-term Southwest Asian population continuity. Within a general pattern of African and Eurasian hominin groups being separated by Pleistocene Saharo-Arabian aridity, our findings reveal the tempo and character of climatically modulated windows for dispersal and admixture.

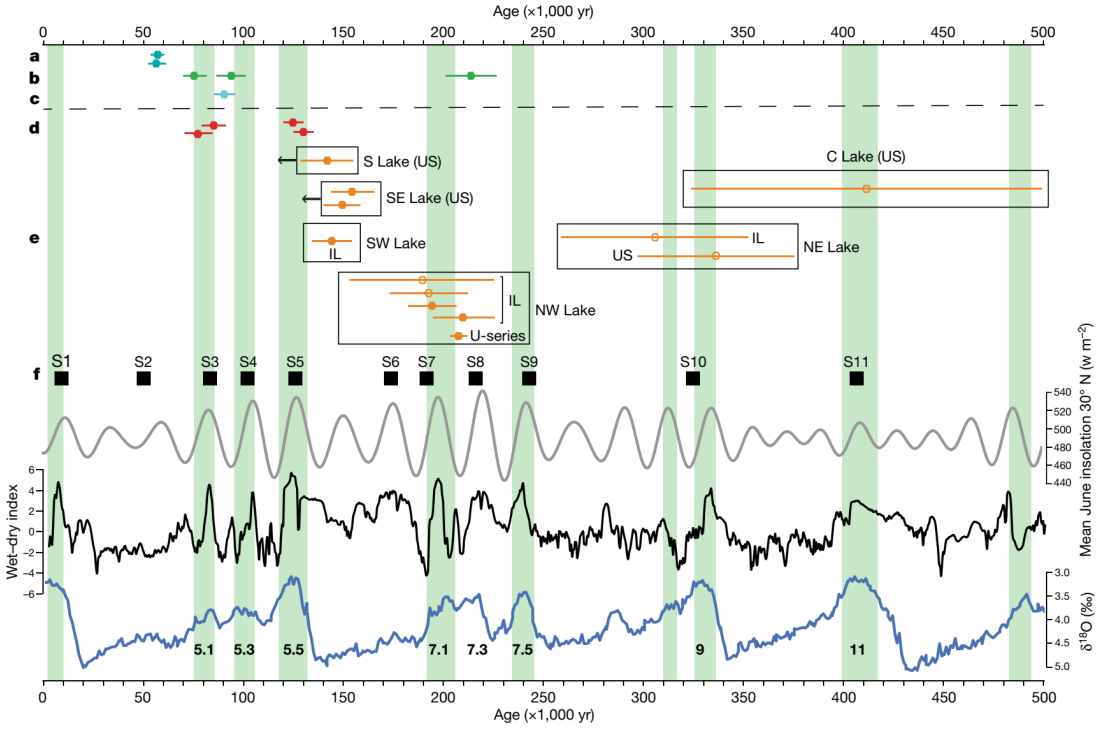

Figure 1. The chronology and environmental context of hominin occupations in northern Arabia. a, Al Marrat 3. b, Jebel-Qattar 1. c, Al Wusta . d, JSM 1 (present study). e, Central (C), Northeast (NE), Northwest (NW), Southwest (SW), Southeast (SE) and South (S) lakes at KAM 4. US, an age for sands underlying the lake (that is, a maximum age for overlying phase of lake formation); IL, in lake (direct date on sediments within lake-related deposits). Black arrows pointing to the left (Southeast and South Lakes) reflect that the luminescence ages provide maximum ages, and the overlying lakes are younger. Filled symbols show quartz ages and open symbols show feldspar ages. f, East Mediterranean sapropel record, insolation (grey), monsoon index (black) and oxygen isotope record (blue). Southern Arabian humid periods are defined by speleothems in green 21. Luminescence ages are presented with 1σ uncertainties and the single U-series age is presented with a 2σ uncertain.

4. 临沧—茵达嫩构造带运动学及 40Ar/39Ar 年代学:对东南亚新生代构造挤出的启示

翻译人：刘伟 inewway@163.com

Wang Y, Wang Y Zhang P, et al. ***Kinematics and $^{40}Ar/^{39}Ar$ geochronology of the Lincang-Inthanon tectonic belt: Implication for Cenozoic tectonic extrusion of SE Asia*** *[J]. GSA Bulletin, 2022.*

https://doi.org/ 10.1130/B36187.1

摘要：临沧—茵达嫩构造带是青藏高原东南部与中南半岛的主要构造边界，是东南亚地区典型的挤出构造。临沧应变带、澜沧江-耿马断裂和茵达嫩变质杂岩构成了这条近南北向的构造带，将宝山地体和思茅-印支地体分开。通过新的岩相学、构造学和云母 $^{40}Ar/^{39}Ar$ 年代学研究，揭示了该构造带变形样式，制约了其构造演化的时间。临沧应变带记录了早渐新世与古特提斯洋俯冲有关的 W—E 向挤压及随后的大陆碰撞和左行韧性剪切作用。澜沧江-耿马断裂带新生代晚期由左旋剪切向右旋剪切转变，其变形历史与平行的红河断裂相似。茵达嫩变质杂岩可能在新生代早期经历了地壳短缩，而后在中新世早期经历了左旋张拉作用。临沧—茵达嫩构造带与高黎贡山、崇山、哀牢山—红河剪切带在岩性、构造演化、变质等方面有许多相似之处。因此，早渐新世以来，沿临沧—茵达嫩构造带和北部崇山构造带的左行剪切作用，对宝山地体和司思茅-印支地体的差异挤压和旋转起了重要的调节作用。我们的研究成果刻画了该区域的构造格架，揭示了印度-欧亚斜向汇聚带东部陆内变形和地球动力学特征。

ABSTRACT: The Lincang-Inthanon tectonic belt is a major tectonic boundary within the southeastern Tibetan Plateau and Indo-China Peninsula, which are typical examples of tectonic extrusion in SE Asia. The Lincang strain zone, Lancang-Gengma fault, and Inthanon metamorphic complex make up this nearly N−S-striking tectonic belt, which separates the Baoshan−Shan Thai and Simao-Indochina terranes. New petrographic, structural, and mica 40Ar/39Ar geochronological studies were conducted to reveal their deformation styles and constrain the timing of their tectonic evolution. W−E-directed compression related to the subduction of the Paleotethyan Ocean with subsequent continental collision and sinistral ductile shearing in the early Oligocene are recorded along the Lincang strain zone. The Lancang-Gengma fault zone switched from sinistral shearing to dextral motion in the late Cenozoic and shows a deformation history similar to that of the parallel

Red River fault. The Inthanon metamorphic complex may have experienced crustal shortening in the early Cenozoic, followed by sinistral transtension in the early Miocene. The Lincang-Inthanon tectonic belt shows many lithological, tectonic evolutionary, and metamorphic similarities with the Gaoligong, Chongshan, and Ailaoshan−Red River shear zones. Therefore, the sinistral shearing along the Lincang-Inthanon tectonic belt and the Chongshan shear zone in the north, which may have initiated since the early Oligocene, played an important role in adjusting differential extrusion and rotation of the Baoshan−Shan Thai and Simao-Indochina terranes. Our results delineate the regional tectonic framework and provide insights into the characteristics and geodynamics of intracontinental deformation in the eastern India-Eurasia oblique convergence zone.

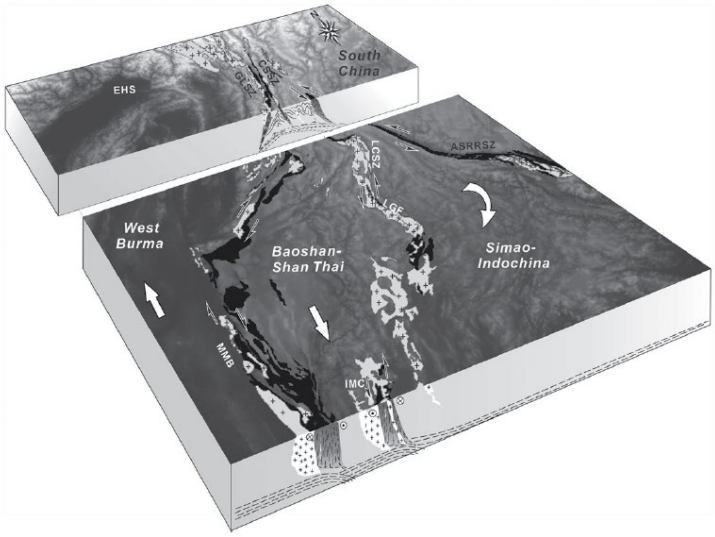

Figure 1. Dynamic model of the SE Tibetan Plateau and Indo-China Peninsula shows differential extrusion and rotation of the Baoshan–Shan Thai and Simao-Indochina terranes, which were adjusted by the sinistral Chongshan–Lincang–Inthanon tectonic belt. EHS—eastern Himalayan syntaxis; MMB—Mogok metamorphic belt; ASRRSZ—Ailao Shan-Red River shear zone;CSSZ—Chongshan shear zone; GLSZ—Gaoligong shear zone; IMC—Inthanon metamorphic complex; LGF—Lancang- Gengma fault; LCSZ—Lincang strain zone.

5. 以色列 Soreq 洞穴石笋中磁性矿物记录的全新世湿润期

翻译人：杨会会 11849590@mail.sustech.edu.cn

Burstyn Y, Shaar R, Keinan J, et al., ***Holocene wet episodes recorded by magnetic minerals in stalagmites from Soreq Cave, Israel [J].*** *Geology, 2021.*

https://doi.org/10.1130/G49383.1

摘要：本研究证实了当石笋生长于半干旱环境中时，石笋磁学作为古水文指标的可行性。石笋中来自土壤的磁性颗粒保留了关于上覆土壤的物理化学条件和基岩水文变化的宝贵信息。然而，石笋磁性指标和同位素指标之间的联系还只是部分建立起来。我们揭示了以色列 Soreq 洞穴中 2 根全新世石笋的磁性矿物输入（定量化指标为 IRM_{flux}）和 $\delta^{13}C$ 之间的关系。石笋记录的时间跨度约为 9.7 ~ 5.4 ka，反映了全新世早期的温湿环境以及向全新世中期干湿循环的过渡。全新世早期极低的 IRM_{flux} 表明上覆土壤的贡献极小，同时伴随着异常高的 $\delta^{13}C$（接近基岩值），推测是由高降雨和土壤侵蚀引起的。全新世中期的 IRM_{flux} 与 $\delta^{13}C$ 和 $\delta^{18}O$ 的锯齿型旋回密切相关，表现为降雨量的快速波动。IRM_{flux} 中的峰值相比负的（湿润）$\delta^{13}C$ 峰值早 60-120 年。这种明显的滞后可以解释为，相对于较慢的土壤有机质周转速率（10-10^2 年），上覆土壤颗粒通过地下水的快速物理转移(高 IRM_{flux} 值)是对降雨增加的响应。

ABSTRACT: This study demonstrates the feasibility of speleothem magnetism as a paleo-hydrology proxy in speleothems growing in semi-arid conditions. Soil-derived magnetic particles in speleothems retain valuable information on the physicochemical conditions of the overlying soil, and changes in bedrock hydrology. Yet, the link between magnetic and isotopic proxies of speleothems has been only partly established. We reveal strong coupling between the inflow of magnetic particles (quantified using the magnetic flux index, IRM_{flux}) and $\delta^{13}C$ in two Holocene speleothems from Soreq Cave (Israel). The stalagmite record spans from ca. 9.7 to ca. 5.4 ka, capturing the warm-humid conditions associated with the early Holocene and the transition to mid-Holocene wet-dry cycles. Extremely low IRM_{flux} during the early Holocene, indicating minimal

contribution from the overlying soil, is accompanied by anomalously high $\delta^{13}C$ (approaching bedrock values) hypothesized to be caused by high rainfall and soil erosion. By contrast, IRM_{flux} during the mid-Holocene covaries with the saw-tooth cyclicity of $\delta^{13}C$ and $\delta^{18}O$, interpreted as rapid fluctuations in rainfall amount. The peaks in IRM_{flux} precede the negative (wet) $\delta^{13}C$ peaks by ~60 - 120 yr. The apparent lag is explained as a rapid physical translocation of overlying soil particles via groundwater (high IRM_{flux}) as a response to increasing rainfall, compared with slower soil organic matter turnover rates ($10–10^2$ yr).

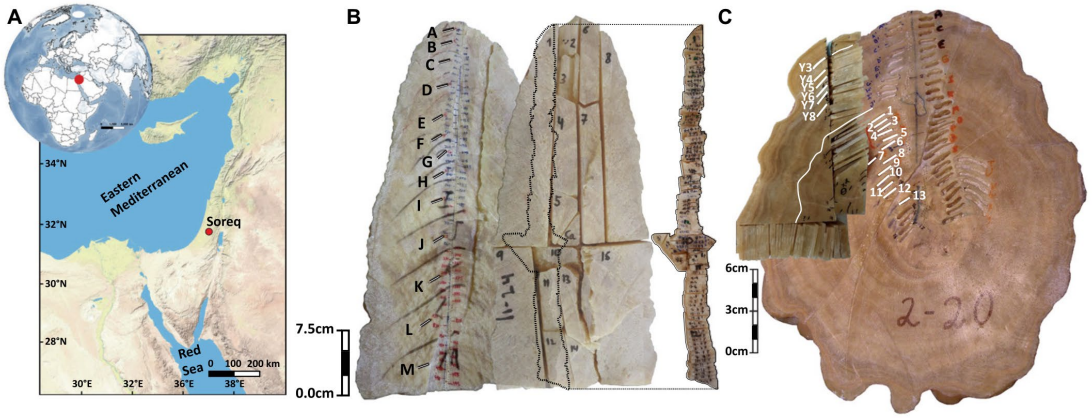

Figure 1. (A) The eastern Mediterranean, with the location of Soreq Cave, Israel (31°45′21″N, 35°01′20″E, WGS84). (B,C) Stalagmites 11-24 and 2-20 superimposed with the slices used for magnetic analysis. Black lines (on 11-24) and white lines (on 2-20) mark the locations of U-Th sampling (denoted by letters and numbers). Small holes (numbered from top to bottom, in intervals of five) mark the stable isotope measurements.

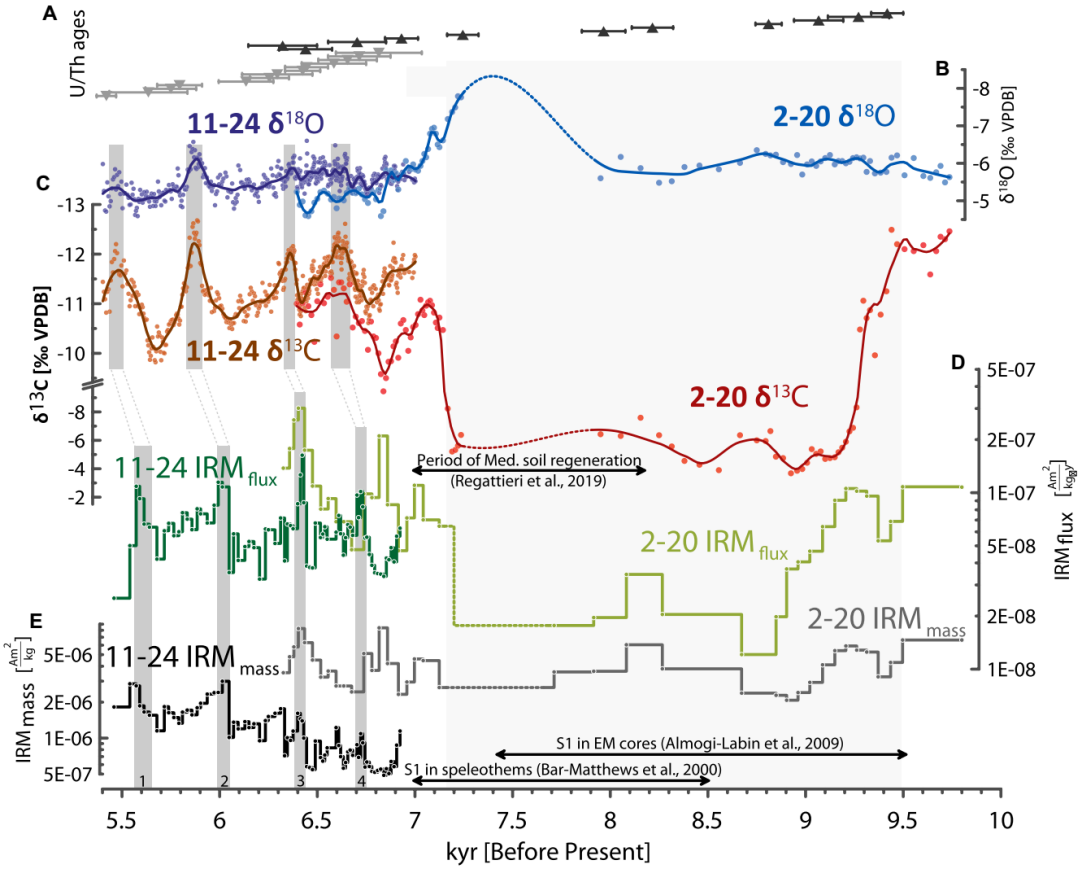

Figure 2. Composite multi-proxy time series of stalagmites 2-20 and 11-24 from Soreq Cave, Israel. (A) U-Th ages used for the age model. (B,C) $\delta^{18}O$ and $\delta^{13}C$ time series superimposed with a locally estimated scatterplot smoothing (LOESS) function with a Gaussian kernel and second order locally weighted polynomial. Light gray shaded area is the isotopic excursion defining sapropel layer S1. Dark-gray vertical bands in C and E highlight four mid-Holocene wet-dry cycles (see text for details). VPDB-Vienna Peedee belemnite. (D,E) Isothermal remanent magnetization normalized to flux (IRM_{flux}) and to mass (IRM_{mass}). Sapropel 1 (S1) timing is marked by black arrowed lines in E and by light-gray shading throughout the plot. Timing of Mediterranean (Med.) soil regeneration in D is marked by black arrowed line (Regattieri et al. (2019).

6. 温暖气候下热带气旋的极向扩张

翻译人：张亚南 yananzhang9@163.com

Studholme S, Fedorov A V, Gulev S K, et al. ***Poleward expansion of tropical cyclone latitudes in warming climates*** *[J]. Nature Geoscience, 2021,15,14-48.*

https://doi.org/10.1038/s41561-021-00859-1

摘要：热带气旋（TCs,也被称为飓风和台风）通常形成于低纬度地区，可以进入到热带海洋的温暖水域，但离赤道足够远，足以让行星旋转导致聚集的对流自旋上升为相干涡旋。然而，目前 TC 纬度的预测框架得出与气候变化相矛盾的预测。对过去温暖时期（如：始新世和上新世）的模拟表明，相比 pre-industrial 环境下 TC 可以在高纬度形成和强化。21 世纪的观测和模型结果表明，由于人为温室气体的排放，TC 可能会再次向极地迁移，这对地球上人口最多的地区构成了深远的风险。由于在数值模拟中难以分辨的原因，以往的研究在很大程度上忽视了单个风暴在时间和空间上的复杂过程。文中，作者在 Hadly 环流，急流和热带辐合带（ITCZ）对全球变暖的响应下重新回顾了这一中尺度物理现象。文中的结论是，21 世纪的 TC 极有可能占据了比过去 3 百万年更广的纬度范围，因为低纬度起源的 TC 将得到中纬度 TC 有利环境的补充，尽管目前的方法还无法对未来的迁移进行精确的估计。

ABSTRACT: Tropical cyclones (TCs, also known as hurricanes and typhoons) generally form at low latitudes with access to the warm waters of the tropical oceans, but far enough off the equator to allow planetary rotation to cause aggregating convection to spin up into coherent vortices. Yet, current prognostic frameworks for TC latitudes make contradictory predictions for climate change. Simulations of past warm climates, such as the Eocene and Pliocene, show that TCs can form and intensify at higher latitudes than of those during pre-industrial conditions. Observations and model projections for the twenty-first century indicate that TCs may again migrate poleward in response to anthropogenic greenhouse gas emissions, which poses profound risks to the planet's most populous regions. Previous studies largely neglected the complex processes that occur at temporal and spatial scales of individual storms as these are poorly resolved in numerical models. Here we

review this mesoscale physics in the context of responses to climate warming of the Hadley circulation, jet streams and Intertropical Convergence Zone. We conclude that twenty-first century TCs will most probably occupy a broader range of latitudes than those of the past 3 million years as low-latitude genesis will be supplemented with increasing mid-latitude TC favourability, although precise estimates for future migration remain beyond current methodologies.

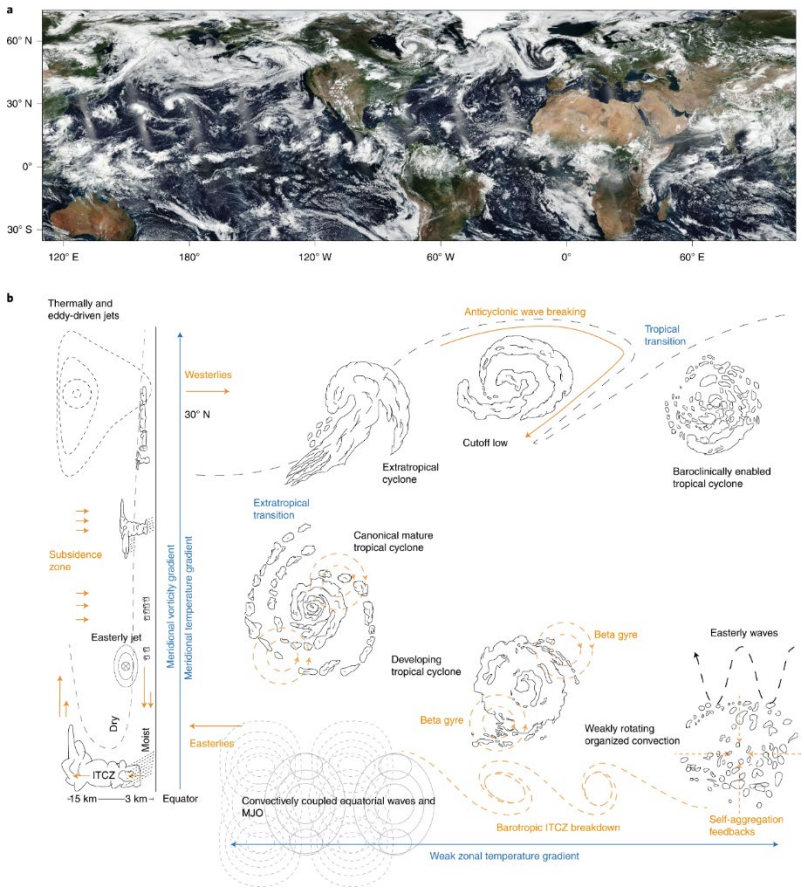

Figure 1. Tropical cyclogenesis in weather and climate. a, Earth's atmosphere on 22 July 2017 from NASA EOSDIS. This day exhibits the most simultaneously existing TCs in the satellite record. Tropical Storms Roke (peak intensity 18 m s^{-1}), Sonca (18 m s^{-1}), Kulap (20 m s^{-1}) and Typhoon Noru (49 m s^{-1}) are seen in the western subtropical North Pacific. In the eastern North Pacific, Hurricane Fernanda (65 m s^{-1}), Tropical Storm Greg (27 m s^{-1}), Hurricane Hilary (49 m s^{-1}) and Hurricane Irwin (40 m s^{-1}) are seen at various development stages. b, Schematic of traditional and baroclinically enabled tropical cyclogenesis embedded into the large-scale flow and atmospheric dynamics (see Extended Data Figs. 1 and 2 for examples). The schematic style of the tropical mean circulation follows that of Bony et al.

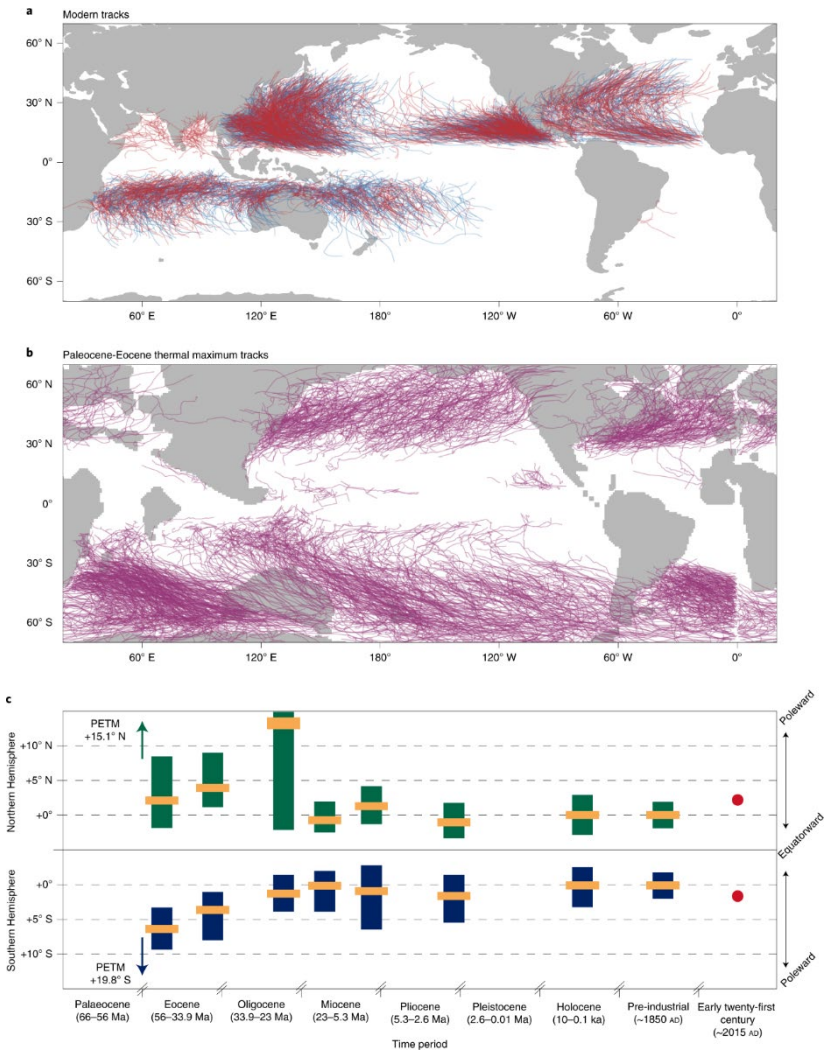

Figure 2. Changes in TC latitudinal distribution over geological timescales. a, Modern TC tracks, the blue curves correspond to the period 1980–1999 and red ones to 2000–2019. b, Simulated PETM TC tracks. c, Changes in simulated seasonal-mean genesis potential relative to pre-industrial throughout the Cenozoic. In c, the yellow strips indicate shifts in the hemispheres' maximum genesis potential latitudes and the green and blue columns mark their upper and lower bounds, respectively (defined as latitudes of 25% drop-offs on either side of the maxima). The data in b and c are based on GCM simulations and hold large uncertainties. Red circles in c indicate the observed satellite era poleward TC migration of the modern era. Pre-industrial TC LMI latitudes are 18° N and 16° S. Given the wide range in twenty-first century projections (see text), no future estimates are plotted.

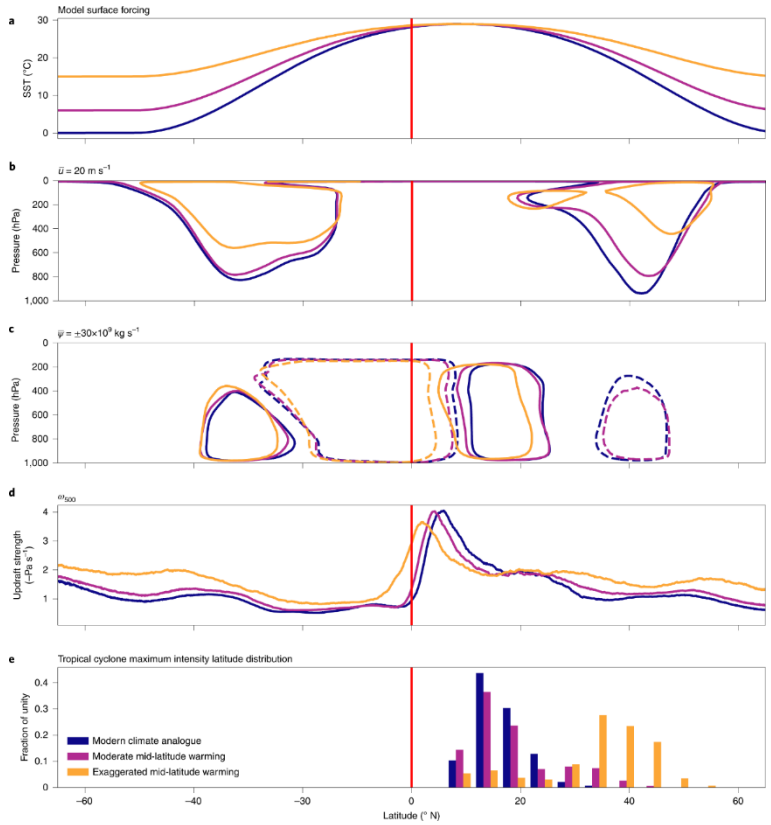

Figure 3. Large-scale circulations and TC latitudinal distributions under idealized climate warming scenarios in cloud-system-resolved aquaplanet simulations. a, The model is forced by three fixed SST meridional profiles that range from contemporary climate (blue) to moderate mid-latitude warming (purple) to exaggerated Eocene-like warming (orange). b, $\bar{u} = 20\ m\ s^{-1}$ zonal velocity contours that mark the jet streams. c, $\bar{\Psi} = \pm 30 \times 109\ kg\ s^{-1}$ streamlines of the Hadley and Ferrel cells. d, Mean updraft strength measured as the time mean of the zonal maximum pressure velocity at 500 hPa multiplied by –1. e, Divergent influences lead to the northward shift of TC LMI distribution (despite non-monotopic changes at low latitudes). Data from Fedorov et al., who also found that GPI calculations underestimate the magnitude of the mid-latitude genesis response to warming.

7. 非洲 4000 年以来的区域地磁场模型

翻译人：李海 12031330@mail.sustech.edu.cn

Di Chiara A, & Pavón-Carrasco F J. ***A first regional model of the past Earth's magnetic field from Africa for the last 4000 years*** *[J]. Physics of the Earth and Planetary Interiors, 2022, 106855.*

https://doi.org/10.1016/j.pepi.2022.106855

摘要: 出于一些原因，理解非洲大陆上地球磁场的变化是至关重要的。例如，目前地磁场最重要的特征--南大西洋异常（SAA），其特征是地磁场强度值低于其维度的预期值，可能在公元第二个千年开始时出现在南非。本研究中，作者遵循 FAIR 原则选择了可用的火山和古地磁数据。然后，使用二维球冠谐波（SCH）分析，构建了第一个过去 4000 年的非洲区域地磁场模型。新的模型显示，自 1100 CE 以来 SAA 从印度洋向西迁移到非洲。此外，该模型可作为非洲地区的古地磁测年工具，可用于确定其他非洲考古遗址以及东非的众多活火山和休眠火山的年代。

ABSTRACT: The understanding of the Earth's magnetic field variations over time on the African continent is fundamental for several reasons. For instance, the most important feature of the present geomagnetic field, the South Atlantic Anomaly (SAA) characterized by weaker geomagnetic strength values than those expected for their latitudes, may have emerged in South Africa at the beginning of the second millennium CE. Here, we first selected the available volcanic and archaeomagnetic data following a set of three criteria inspired by the FAIR principles. We then built a first regional geomagnetic model for Africa covering the last 4000 years, using a revised version of the spherical cap harmonic (SCH) analysis in 2 dimensions. The new regional model shows, at the Earth's surface, the westward migration of the SAA from the Indian Ocean over Africa since 1100 CE. In addition, the regional model is tested as a paleomagnetic dating tool by re-dating previous archaeomagnetic data from Africa and thus can be used to date other African archeological sites and the numerous active and dormant

volcanoes of the East African System.

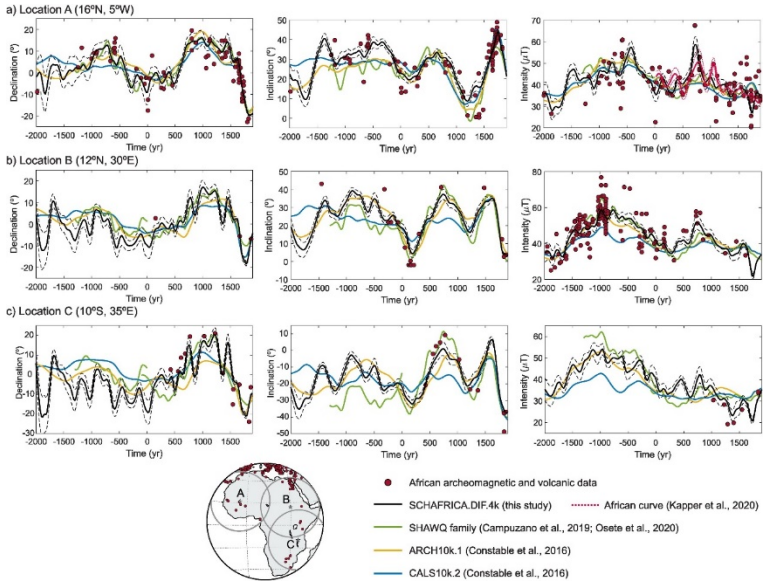

Figure 1. Paleosecular variation curves at three different locations from the SCHAFRICA.DIF.4 k regional model (black curves and their associated 1σ error as black dashed lines) and from global models (blue and yellow lines are the CALS10k.2 and ARCH10k.1 models of Constable et al., 2016; green lines refer to the SHAWQ family models of Campuzano et al., 2019; Osete et al., 2020). For comparison, all the available archeomagnetic and volcanic data (red dots) for the three African regions are also plotted. The inset map indicates the location of the three regions, A, B and C. (For interpretation of the references to colour in this figure legend, the reader is referred to the web version of this article.)

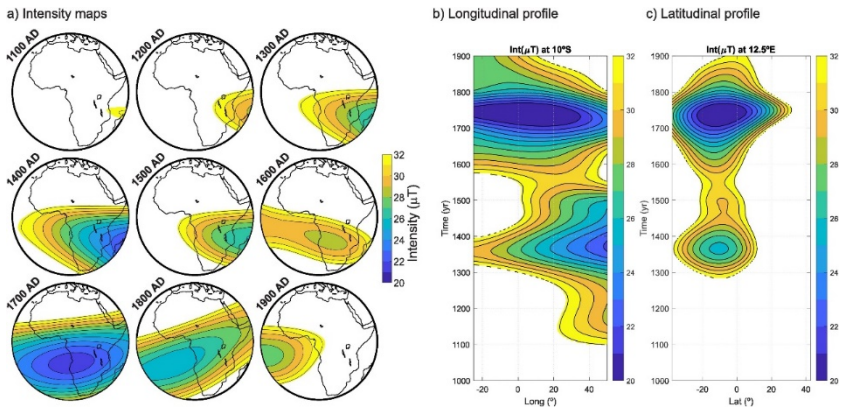

Figure 2. a) Intensity snapshot maps from the SCHAFRICA.DIF.4 k model every 100 yrs. from 1000 to 1900 CE. Hovmöller diagrams of East-West (b) and South-North (c) profiles of the intensity element for the last millennium. Only the isodynamic lines below 32 μT are shown in both maps and Hovmöllers to reveal the past evolution of the SAA over the last millennium.

8. 祝融火星巡视器行进路线上乌托邦平原表面特征

翻译人：张伟杰 12031188@mail.sustech.edu.cn

Ding L, Zhou R, Yu T, et al. ***Surface characteristics of the Zhurong Mars rover traverse at Utopia Planitia****[J]. Nature Geoscience, 2022, 1-6.*

https://doi.org/10.1038/s41561-022-00905-6

摘要：2021 年五月中国祝融号火星车在火星北部低地乌托邦着陆并已经开始与天文一号轨道飞行器联合在着陆区开展原位调查。本文，我们展示了祝融巡视器在前 60 个火星日运行过程中所获得的火星表面特性。我们根据这段时间的运动数据和相机图像分析了巡视器的位置，巡视器在车轮轻微打滑的平面上向南行驶了 450.9 米。通过观察轮-地相互作用的地面力学参数确定了表土的承载强度和黏聚力。土壤的等效刚度估计范围为 1390～5872 kPa / mN，黏聚力为 1.5～6kpa 时，内摩擦角为 21°～34°。该地区的风成底型主要为横向风成脊，表明了当地的东北风向。巡视器相机拍摄的地表岩石显示出风蚀等物理风化过程的证据和潜在的化学风化过程。利用巡视器和轨道器的科学有效载荷进行联合调查，可以深入了解当地的风成历史和水成历史，以及火星北部低地的宜居性演变。

ABSTRACT: China's Mars rover, Zhurong, touched down on Utopia Planitia in the northern lowlands of Mars (109.925° E, 25.066° N) in May 2021, and has been conducting in situ investigations of the landing area in conjunction with the Tianwen-1 orbiter. Here we present surface properties derived from the Zhurong rover's traverse during the first 60 sols of rover operations. Our analysis of the rover's position from locomotion data and camera imagery over that time shows that the rover traversed 450.9 m southwards over a flat surface with mild wheel slippage. Soil parameters determined by terramechanics, which observes wheel–terrain interactions, indicate that the topsoil has high bearing strength and cohesion. The soil's equivalent stiffness is estimated to range from 1,390 to 5,872 kPa per mN, and the internal friction angle ranges from 21° to 34° under a cohesion of 1.5 to 6 kPa. Aeolian bedforms in the area are primarily transverse aeolian ridges, indicating northeastern local wind directions. Surface rocks imaged by the rover cameras show evidence of physical weathering processes, such as wind erosion, and potential chemical weathering

processes. Joint investigations utilizing the scientific payloads of the rover and the orbiter can provide insights into local aeolian and aqueous history, and the habitability evolution of the northern lowlands on Mars.

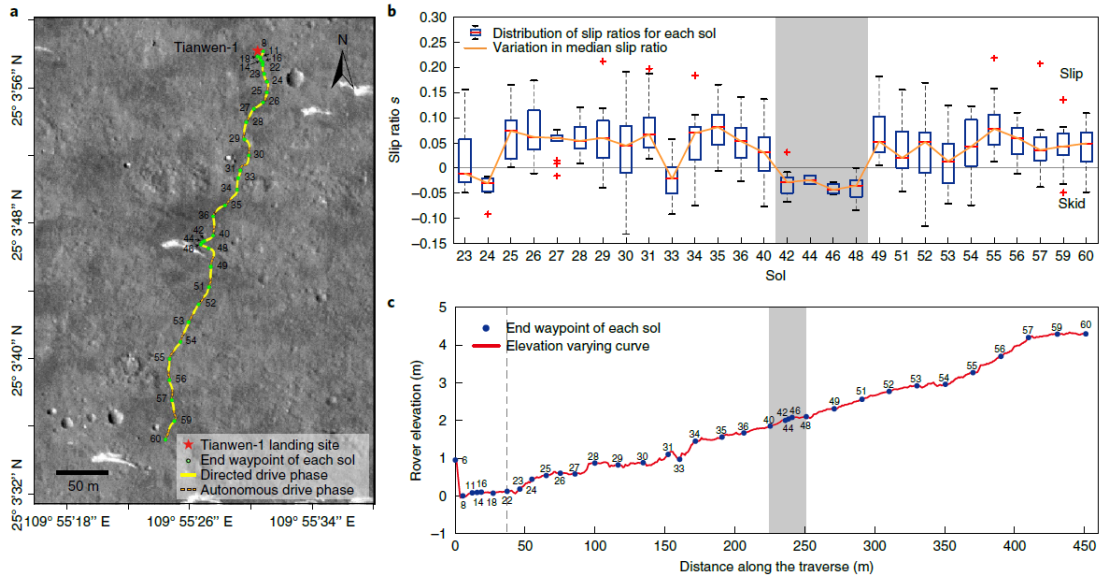

Figure 1. The routing path of the Zhurong rover and the associated wheel slippage for the first 60 sols. a, The routing path of the Zhurong rover. The green dots represent the end waypoint on each sol. The base image is a high-resolution (0.7 m pixel−1) digital orthophoto map generated by the HiRIC9. Image credit: CNSA/BACC. b, Boxplot of Zhurong rover's wheel slip ratios when moving in high-efficiency mode (from sol 23 onwards). The lower and upper bounds of each box represent the first and the third quartile of slip ratios on that sol, respectively. The red line inside each box represents the statistical median of slip ratios. The lower and upper whiskers of each box represent the minimum and maximum of slip ratios experienced on that sol. The red crosses represent outliers of slip ratios. Travelling distances on sols 42–48 (grey shading) are short, causing relatively large locomotion measurement errors and resulting in the slip ratio being in disagreement with the elevation trend. c, The rover elevation along the traversed path. The blue dots represent the rover elevation at end waypoints on each sol. The grey dashed line divides the traverse according to the work mode, and the right side of the grey dashed line is the traverse performed under the high-efficiency mode. The grey-shaded area is the traverse on sols 42–48. The rover elevation at the end waypoint of sol 8 (the initial waypoint on the surface) is taken as the baseline (elevation of 0), and the elevation varies from 0 m (on sol 8) to 4.34 m (on sol 60).

9. 白垩纪超静磁带：对其发现、短反转事件、古强度、长期变化、古环境、火山作用和机制的简评

翻译人：王浩森 11930841@mail.sustech.edu.cn

Yoshimura Y. ***The Cretaceous Normal Superchron: A Mini-Review of Its Discovery, Short Reversal Events, Paleointensity, Paleosecular Variations, Paleoenvironment, Volcanism, and Mechanism****[J]. Frontiers in Earth Science, 2022, 10, 834024.*

https://doi.org/10.3389/feart.2022.834024

摘要：白垩纪超静磁带（CNS）最早定义于 20 世纪 60 年代，用于解释海洋磁异常剖面中不包括或极少地磁反转的白垩纪平静带。这个 3700 万年的时段被认为是过去 160Myr 中最独特和极端的地磁特征。超静磁带可能是由在核幔边界（CMB）以独特的热通量并以峰值效率运行的地球动力因素引起的。之前的研究表明，超静磁带是地球内部和表面之间联系的标志。在 CNS 期间，地磁强度可能发生显著波动，平均值可能随时间而变化，地磁场长期变化具有独特的特征。CNS 时期的温暖气候可能是由与活跃地幔对流相关的火山活动造成的。这种地幔对流增加了 CNS 期间 CMB 的热通量，但与地球动力模拟预测的热通量较小是不一致的。这种差异可能是通过超级地幔柱的增长和崩溃或俯冲通量的增加和减少来解释。

ABSTRACT: The Cretaceous Normal Superchron (CNS) was first defined in the 1960s to explain the Cretaceous Quiet Zone in marine magnetic anomaly profiles, which includes no or fewer geomagnetic reversals. This ~37 million years period is considered the most unique and extreme geomagnetic feature for the last 160 Myr. Superchrons may be caused by the geodynamo operating at peak efficiency with a unique heat flux at the core-mantle boundary (CMB). Previous studies suggest that the CNS is a sign of the connection between Earth's interior and surface. During the CNS, the geomagnetic intensity may have fluctuated significantly, and the average may have changed with time, and the paleosecular variations had unique features. The warm climate around the CNS may have been caused by volcanic activity associated with active mantle convection. Such mantle convection increases heat flux at the CMB during the CNS, but geodynamo simulations

predict small heat flux, which are inconsistent. This discrepancy may be resolved by the growth and collapse of a superplume or by an increase and decrease in the subduction flux.

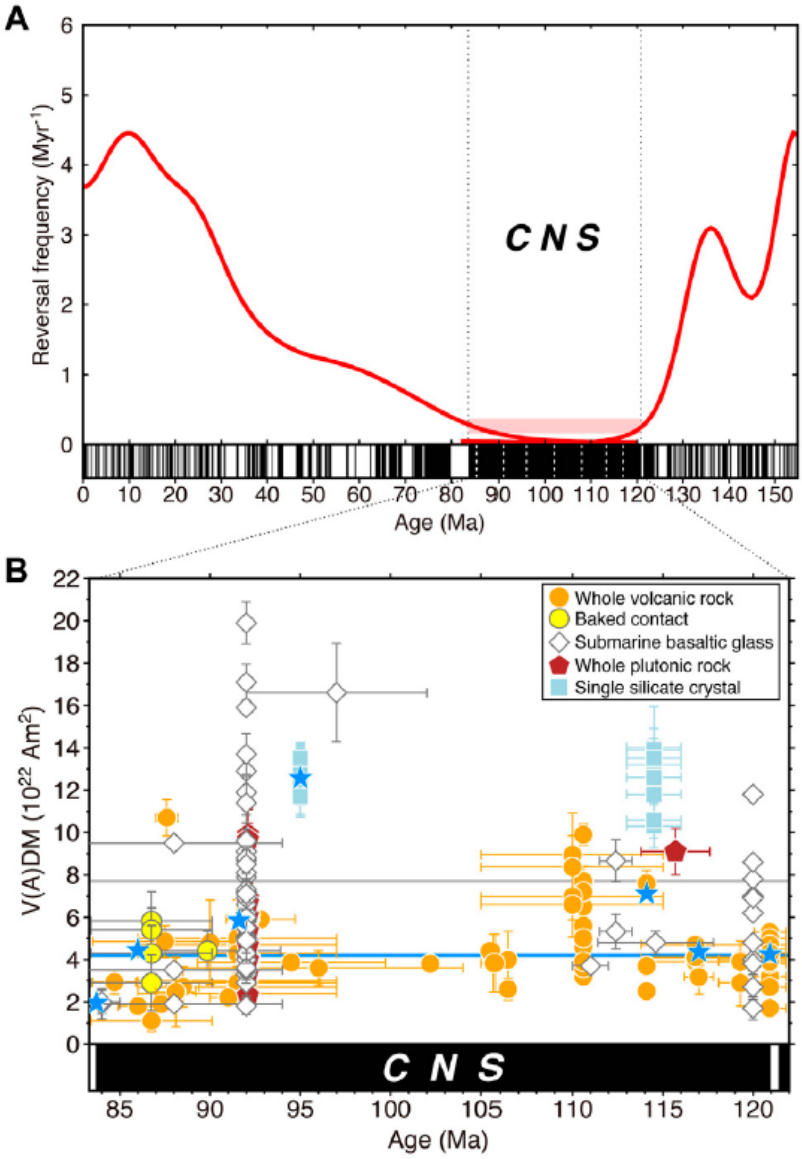

Figure 1. (A) Geomagnetic polarity time scale for 0–154.9 Ma and geomagnetic reversal frequency curve calculated using fixed kernel density estimation. Possible short geomagnetic reversal events during the CNS are shown as dashed white lines. Note that the duration of the events are not reflected in this figure. Constable (2000) calculated the reversal frequency from Harland et al. (1990) and Cande and Kent (1995). Pink zone expresses a range of the geomagnetic reversal frequency during the CNS (Chron C34n) calculated from short geomagnetic reversal events during the Superchron suggested by Zhang et al. (2021). Dotted gray lines express a time interval of the CNS.

The CNS, Cretaceous Normal Superchron. (B) Virtual (axial) dipole moments during the CNS.

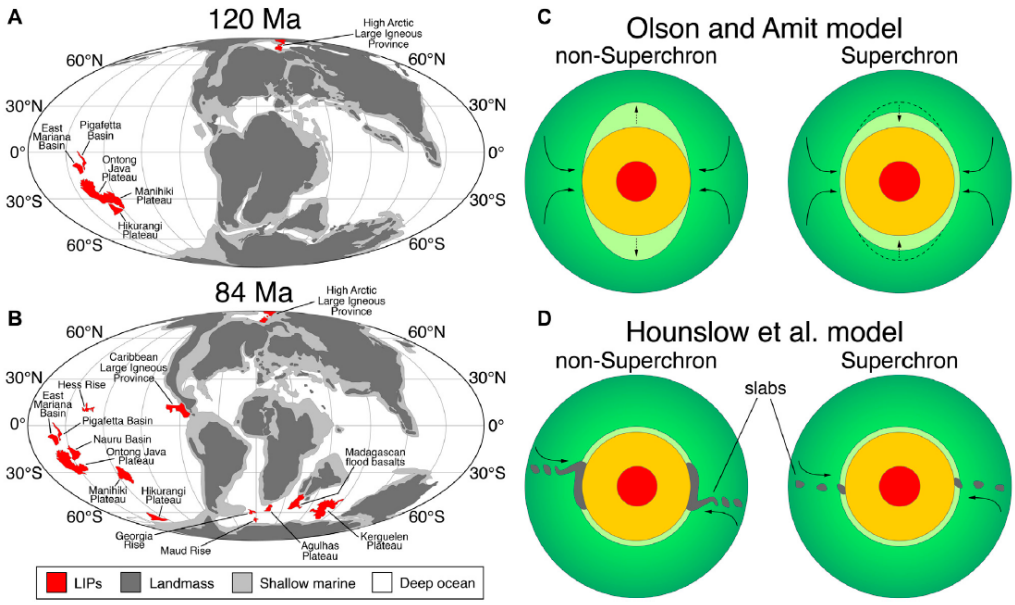

Figure 2. (A,B) Distribution of Large Igneous Provinces at 120 Ma (A) and 84 Ma (B) with paleogeography based on Johansson et al. (2018), which erupted during the CNS. LIPs, Large Igneous Provinces. (C,D) Two hypotheses for the cause of the CNS. (C) Equatorial cross-sections of the core (red and orange) and lower mantle (green) illustrating superplume growth and collapse in the D″-region (light green) above the core-mantle boundary based on Olson and Amit (2015). Arrows indicate the lower mantle circulation patterns. Superplume growth thins the D″-region below lower mantle downwelling, which increases the heat flux average at the core-mantle boundary. The geodynamo expresses a higher geomagnetic reversal frequency at that time. On the contrary, superplume collapses reduces the heat flux average at the core-mantle boundary and reduce reversal frequency, which is Superchron. (D) Cross-sections of the core (red and orange) and lower mantle (green) illustrating changing of the subduction flux (the volume of slabs) based on Hounslow et al. (2018), which reaches the D″ layer (light green) above the core-mantle boundary. Higher subduction flux increases the volume of slabs reaching the D″ layer, increases the heat flux average at the core-mantle boundary, and increases geomagnetic reversal frequency. On the contrary, lower subduction flux reduces the volume of slabs reaching the D″ layer, reduces the heat flux average at the coremantle boundary, and reduces reversal frequency, which is Superchron